



**HAL**  
open science

## Co-Clustering of Multivariate Functional Data for the Analysis of Air Pollution in the South of France

Charles Bouveyron, Julien Jacques, Amandine Schmutz, Fanny Simoes, Silvia Bottini

► **To cite this version:**

Charles Bouveyron, Julien Jacques, Amandine Schmutz, Fanny Simoes, Silvia Bottini. Co-Clustering of Multivariate Functional Data for the Analysis of Air Pollution in the South of France. 2020. hal-02862177v1

**HAL Id: hal-02862177**

**<https://hal.science/hal-02862177v1>**

Preprint submitted on 9 Jun 2020 (v1), last revised 14 Sep 2021 (v2)

**HAL** is a multi-disciplinary open access archive for the deposit and dissemination of scientific research documents, whether they are published or not. The documents may come from teaching and research institutions in France or abroad, or from public or private research centers.

L'archive ouverte pluridisciplinaire **HAL**, est destinée au dépôt et à la diffusion de documents scientifiques de niveau recherche, publiés ou non, émanant des établissements d'enseignement et de recherche français ou étrangers, des laboratoires publics ou privés.

# Co-Clustering of Multivariate Functional Data for the Analysis of Air Pollution in the South of France

C. Bouveyron<sup>1</sup>, J. Jacques<sup>2</sup>, A. Schmutz<sup>2</sup>, F. Simões<sup>3</sup> & S. Bottini<sup>3</sup>

<sup>1</sup> Université Côte d'Azur, Inria, CNRS, LJAD, Maasai, Nice, France

<sup>2</sup> Université de Lyon, Lyon 2, Laboratoire ERIC, EA 3083, Lyon, France

<sup>3</sup> Université Côte d'Azur, MSI, Nice, France

June 9, 2020

## Abstract

Air pollution is nowadays a major treat for public health, with clear links with many diseases, especially cardiovascular ones. The spatio-temporal study of pollution is of great interest for governments and local authorities when deciding for public alerts or new city policies against pollution raise. The aim of this work is to study spatio-temporal profiles of environmental data collected in the south of France (Région Sud) by the public agency AtmoSud. The idea is to better understand the exposition to pollutants of inhabitants on a large territory with important differences in term of geography and urbanism. The data gather the recording of daily measurements of five environmental variables, namely three pollutants (PM10, NO<sub>2</sub>, O<sub>3</sub>) and two meteorological factors (pressure and temperature) over six years. Those data can be seen as multivariate functional data: quantitative entities evolving along time, for which there is a growing need of methods to summarize and understand them. For this purpose, a novel co-clustering model for multivariate functional data is defined. The model is based on a functional latent block model which assumes for each co-cluster a probabilistic distribution for multivariate functional principal component scores. A Stochastic EM algorithm, embedding a Gibbs sampler, is proposed for model inference, as well as a model selection criteria for choosing the number of co-clusters. The application of the proposed co-clustering algorithm on environmental data of the Région Sud allowed to divide the region composed by 357 zones in six macro-areas with common exposure to pollution. We showed that pollution profiles vary accordingly to the seasons and the patterns are conserved during the 6 years studied. These results can be used by local authorities to develop specific programs to reduce pollution at the macro-area level and to identify specific periods of the year with high pollution peaks in order to set up specific prevention programs for health. Overall, the proposed co-clustering approach is a powerful resource to analyse multivariate functional data in order to identify intrinsic data structure and summarize variables profiles over long periods of time.

*Keywords:* latent block model, multivariate functional data, SEM-Gibbs algorithm, pollution, co-clustering.

# 1 Introduction

There is a growing body of evidence that air pollution is a significant threat to health worldwide (WHO, 2013). Air pollution is composed of particulate matter (PM) and gaseous pollutants, such as nitrogen dioxide (NO<sub>2</sub>) and ozone (O<sub>3</sub>) (IAR, 2016). The time exposure to air pollution leads diverse impact on the health. A short-term exposure to an intense pollution event increases hospital admission and mortality rate, causing mainly respiratory and cardiovascular diseases (Benbrahim-Tallaa L, 2012),(Hamra GB, 2014); whereas a long-term exposure reduces life expectancy (Lelieveld, 2015),(Mathilde Pascal, 2016). Although PM and NO<sub>2</sub> are mainly produced by human activities such as fossil fuel combustion, biomass burning due to agricultural activities, traffic, heating/cooling systems, industrial activities in general; O<sub>3</sub> is a secondary product, meaning that it is not directly produced by human activities. It is naturally produced in the stratosphere when highly energetic solar radiation strikes molecules of oxygen, O<sub>2</sub>, and cause the two oxygen atoms to split apart in a process called photolysis. The Région Sud is an ideal context for the accumulation of this pollutant, regardless the urbanization/industrialization of the subareas, and because of the meteorological conditions: prolonged sun days and rare rain events all over the year, especially in summer, where this pollutant is already at the highest levels. Air pollution is a major concern not only in big cities but also in territories with medium-sized cities and mountainous zones. Mass of air moves from high pressure zones to low pressure and vice versa, thus particulate matter can be moved from one zone to another along with the mass of air, may exposing rural zones to pollution generated by adjacent industrial zones. Hence pollution trend in specific zones do not depend only by the local pollution production, but it is influenced by surrounding zones and meteorological factors. The understanding of air pollution and its spatio-temporal dynamic is of great interest for governments and local authorities in order to set up new city policies to lower down pollution or for public alerts when pollution raise above secure levels for the citizens. However, studies usually focus on isolated cities and do not take into account meteorological features, making their conclusions weak or not representative to generate prediction models. The main limitation is due to the absence of powerful statistical or mathematical models able to analyse the complex spatio-temporal dynamic of pollution in big zones. Here we chose as model the Région Sud in the south of France, to present a novel statistical method to study the behavior of multi-variate variables in order to understand pollution dynamic in this region. This study shows the ability of our co-clustering approach to identify intrinsic structures in these complex data that well suits to describe and analyse pollution behavior. Our results will allow local authorities to set up pollution politics adapted to the heterogeneous territory of the region and will give an instrument to analyse environmental data that can be expanded to other regions/countries.

## 1.1 The Région Sud and the AtmoSud Agency

The Région Sud (formerly known as Provence-Alpes-Côte d'Azur) covers a territory of 31,400 km<sup>2</sup> between Marseille, Nice and Gap, and hosts more than 5 millions of inhabitants. It has a wide variety of landscapes, from the Alps mountains to plains and coastal areas hosting big cities like Nice and Marseille. Most of the population of the region lives in the Mediterranean coastline on the south. The wide variety of landscapes and the imbalance of the population distribution all over the territory, make difficult the study and the modeling of air pollution. Thus, the French Ministry of the Environment in 2012 created the AtmoSud agency to monitor the air quality in the Région Sud. Among its tasks, AtmoSud fulfills a mission of public interest by informing and educating citizens, the State, communities and economic actors about pollution trends offering decision support to implement the most relevant actions to improve air quality. AtmoSud relies on a set of eighty fix and mobile sensors (see sensor locations in Figure 1) which measure several pollutants and meteorological variables. Based on these daily measurements, AtmoSud is able to release every day a detailed map of the pollutants and pollution forecast for the coming days, with a resolution of 4 km, using the sophisticated model Chimere (Menut and Vivanco, 2013) to interpolate sensor measurements.

In the present study, we collected environmental data from AtmoSud agency, specifically daily pollution and meteorological factors measurements for the period from 2013 to 2018 including: the maximum daily value observed for NO<sub>2</sub> and O<sub>3</sub>, the daily average value of PM10 and of maximal and minimal observed temperature (T) and pressure (P) for each of the 357 zones of the Région Sud. Figures 2 and 3) show a sample of the data.

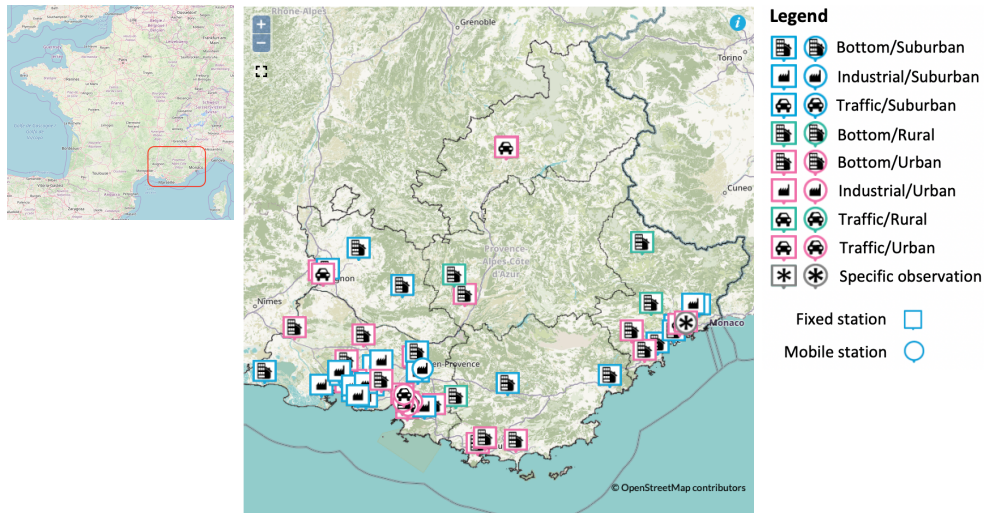


Figure 1: Map of the Région Sud and the locations of the pollution sensors.

## 1.2 Functional co-clustering

The aim of this work is to study the environmental database, constituted by 3 pollution and 2 weather-related variables, in order to identify spatio-temporal clusters representing peculiar pollution trends. Such data can be seen as multivariate functional data: multiple quantitative entities evolving during time collected simultaneously for the same individual (Ramsay and Silverman, 2005; Jacques and Preda, 2014b). In order to analyze and understand multivariate data, we propose to identify subgroups of individuals (i.e. zones, in the present work) that have the similar profiles for each of the 5 variables. However, the large amount of data due to the long time period taken into account in this work could make hard the analysis and the data interpretation. Thus, we split the 6 years in weeks of 7 days. Consequently, for each variable we built a big matrix with 357 rows (zones) and 313 columns (weeks), in which each element is a 5-variate curve. To analyze such massive data, we propose to simultaneously cluster the rows into homogeneous groups of zones and the columns into homogeneous groups of weeks. Such kind of analysis is known as co-clustering (Govaert and Nadif, 2013). The co-clustering will identify homogeneous blocks of cities and weeks having a similar behavior according to the different environmental variables.

In the statistics and machine learning literature, methods for the co-clustering of rows and columns of a data matrix can be split into two main categories: deterministic approaches (see for instance George and Merugu, 2005; Banerjee et al., 2007; Wang and Huang, 2017) and model-based approaches (Govaert and Nadif, 2013; Bouveyron et al., 2019). The selection of the number of row and column clusters is one of the most important tasks in co-clustering analysis and model-based approaches provide a well defined framework for model selection. Moreover, model-based approaches are usually very flexible: taking into account for groups of different sizes, they allow to manage different types of data. All these reasons prompted us to employ the model-based point of view.

One of the most famous model for co-clustering is the latent block model (LBM, (Govaert and Nadif, 2013)). According to the LBM, the elements of a block are modeled by a parametric distribution. Each block is therefore interpretable thanks to the block-distribution's parameters. Moreover, model selection criteria, such as the ICL criterion (Biernacki et al., 2000), can be used for model selection purposes, including the choice of the number of co-clusters. This technique proved its efficiency for co-clustering of several types of data: continuous (Nadif and Govaert, 2008), nominal (Bhatia et al., 2014), binary (Laclau et al., 2017), ordinal (Jacques and Biernacki, 2018; Corneli et al., 2019), functional data (Bouveyron et al., 2017; Chamroukhi and Biernacki, 2017; Slimen et al., 2018) or





Figure 2: Daily distribution of pollutants in Marseille (red) and Nice (blue) for the year 2018: maximum of NO<sub>2</sub> (A) and of O<sub>3</sub> (B) and the average of PM<sub>10</sub> (C).

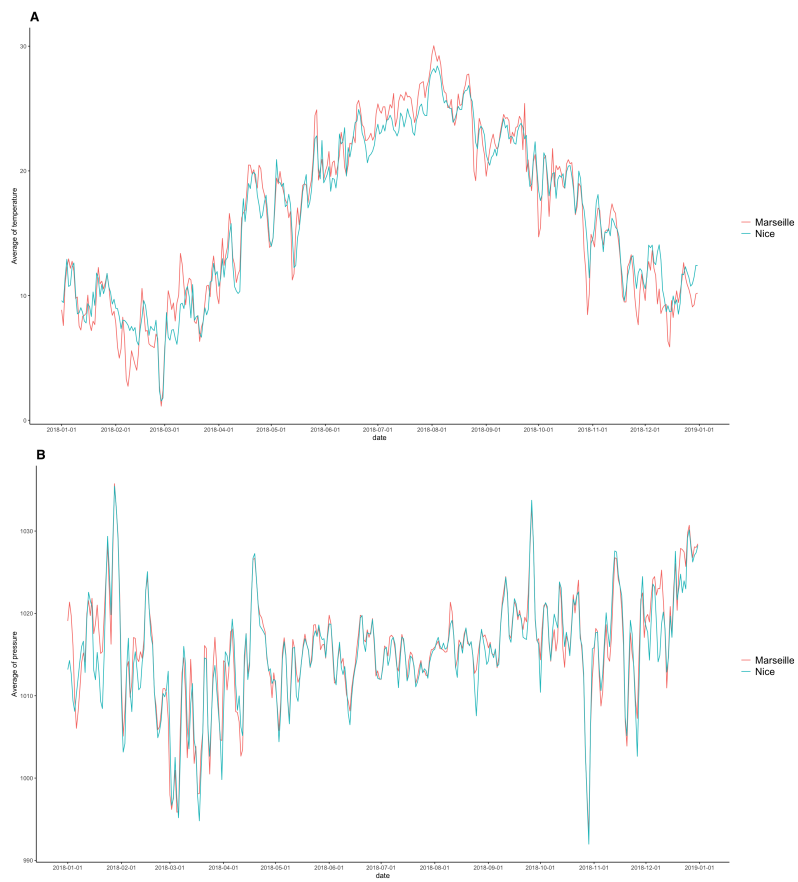


Figure 3: Daily distribution of meteorological factors in Marseille (red) and Nice (blue) for the year 2018: average of temperature (A) and average of pressure (B).

even mixed-type data (Selosse et al., 2019).

Since our database is composed by functional variables, from now on we focus on functional data. Slimen et al. (2018) proposed a co-clustering algorithm based on a vectorial LBM applied on the functional principal components scores of the curves. Bouveyron et al. (2017) extended this work by proposing a functional latent block model assuming that the functional principal components of the curves are block-specific and live into a low-dimensional subspace. Chamroukhi and Biernacki (2017) presented another co-clustering model based on a latent block model where the probability density function is estimated thanks to a regression model with a hidden logistic process. Unfortunately, all these works are designed for univariate functional data and are not able to handle in an appropriate way the multivariate functional data that we consider in this study.

### 1.3 Contributions and organization of the work

In the present work, a co-clustering algorithm for multivariate functional data is proposed to handle the environmental data of the Région Sud that we collected thanks to the AtmoSud agency. The proposed algorithm, named *multiFunLBM*, extends to the multivariate case the methodology proposed by Bouveyron et al. (2017). A SEM-Gibbs algorithm is derived for model inference and a model selection criterion is proposed for choosing the hyper-parameters. The application of the *multiFunLBM* algorithm to the AtmoSud data allowed to identify six spatio-temporal clusters that represents sub groups of zones and weeks with specific pollution trends.

The paper is organized as follows. Section 2 presents the co-clustering model and Section 3 is devoted to model inference. An experimental study of the algorithm on simulated data is presented in Section 4. Section 5 is dedicated to the analysis of the environmental database of the South of France. Some concluding remarks and further work are finally discussed in Section 6.

## 2 A co-clustering model for multivariate functional data

This section introduces a generative model for co-clustering multivariate functional data, such as the ones of AtmoSud.

### 2.1 Data and functional reconstruction

Functional data, which are the observations of a random variable living into an infinite dimensional space, are in practice observed only at a finite set of time points. Let  $\mathbf{x} = (\mathbf{x}_{ij})_{1 \leq i \leq n, 1 \leq j \leq p}$  be the data matrix of dimension  $n \times p$ , where each element  $\mathbf{x}_{ij}$  is a multivariate curve  $\mathbf{x}_{ij} = (x_{ij}^1(t), \dots, x_{ij}^S(t))$  with  $t \in [0, T]$ . Let us denote by  $i$  the row index, by  $j$  the column index and let  $s$  index the dimension of the multivariate curves. In our application,  $i$  refers to the cities (identified by postal codes,  $n = 357$ ),  $j$  refers to a week of the study ( $p = 313$ ) and  $s$  refers either to some pollutant or weather-related variable ( $S = 5$ ). Note that the model and its inference that are presented in this work can be nevertheless used for any other similar set of multivariate functional data.

In practice, the functional expressions of the curves  $x_{ij}^s(t)$  are not known and we only have access to discrete observations at a finite set of times:  $\{x_{ij}^s(t_1), x_{ij}^s(t_2), \dots\}$ . A common way to reconstruct the functional form is to assume that the observations can be decomposed into a finite dimensional space spanned by a basis of functions. So each observed curve  $x_{ij}^s$  ( $1 \leq i \leq n, 1 \leq j \leq p, 1 \leq s \leq S$ ) can be expressed as a linear combination of basis functions  $\{\phi_r^s\}_{r=1, \dots, R_s}$ :

$$x_{ij}^s(t) = \sum_{r=1}^{R_s} c_{ijr}^s \phi_r^s(t) \quad (1)$$

with  $R_s$  the number of basis functions used to reconstruct the  $s$ th functional variable. These basis functions can be for instance Fourier or spline bases. It is worth noticing that the choice of the most appropriate basis (as well as the number of basis functions) is an open problem (Jacques and Preda, 2014a). In practice, this choice is done empirically such that the reconstruction is judged reasonable by the expert. Estimation of the basis expansion coefficients  $c_{ijr}^s$  is classically done by least squares

smoothing. We refer the reader to Ramsay and Silverman (2005) for a complete survey on this aspect.

Let  $c = (c_{ij})_{ij}$  be the whole set of coefficients, which contains the coefficients for the row  $i$  and column  $j$  which corresponds to the concatenation of coefficients  $c_{ijr}^s$  for all  $S$  functional variables, such that  $c_{ij} = (c_{ij1}^1, \dots, c_{ijR_1}^1, \dots, c_{ij1}^S, \dots, c_{ijR_S}^S)^t$ .

For the sake of presentation clarity, the same number of basis functions,  $R_s = R, \forall s = 1, \dots, S$ , and the same basis functions,  $\{\phi_{rs}\}_{r=1, \dots, R} = \{\phi_r\}_{r=1, \dots, R}, \forall s = 1, \dots, S$ , are considered hereafter for each dimension of the multivariate functional variables. Extension is straightforward. Let consequently  $\phi(t)$  be the  $S \times SR$  matrix that gathers basis functions of all  $S$  functional variables:

$$\phi(t) = \begin{pmatrix} \phi_1(t) & \dots & \phi_R(t) & 0 & \dots & 0 & \dots & 0 & \dots & 0 \\ 0 & \dots & 0 & \phi_1(t) & \dots & \phi_R(t) & \dots & 0 & \dots & 0 \\ \dots & \dots & \dots & \dots & \dots & \dots & \dots & \dots & \dots & \dots \\ 0 & \dots & 0 & 0 & \dots & 0 & \dots & \phi_1(t) & \dots & \phi_R(t) \end{pmatrix}.$$

With these notations, Equation 1 can be written in matrix terms:

$$x_{ij}(t) = \phi(t)c_{ij}. \quad (2)$$

It is worth noticing that, depending on the basis function choice, the basis functions may not be orthonormal, *i.e.*  $\Phi = \int_0^T \phi(t)^t \phi(t) dt$  may not be the identity matrix. This is in particular the case when considering B-splines or polynomial functions. Conversely, Fourier basis functions are by construction such that  $\Phi = I$ . In any case, it is of course possible to express the expansion coefficients within an orthonormal basis function system:

$$x_{ij}(t) = \psi(t)\Phi^{1/2}c_{ij}, \quad (3)$$

where  $\psi(t) = \phi(t)\Phi^{-1/2}$ . Thus, the expansion coefficients of  $x_{ij}(t)$  within the orthonormal basis  $\{\psi_1(t), \dots, \psi_M(t)\}$  are  $\Phi^{1/2}c_{ij}$ , where  $M = S \times R$ .

## 2.2 The proposed latent block model

The aim of a co-clustering model is to define row and column partitions in order to summarize the data matrix  $x$  into smaller subgroups, usually called blocks, that are eventually distributed in the same way. To this end, let  $z = (z_{ik})_{1 \leq i \leq n, 1 \leq k \leq K}$  be the row partition of the  $n$  rows into  $K$  groups, and  $w = (w_{jl})_{1 \leq j \leq p, 1 \leq l \leq L}$  the column partition of the  $p$  columns into  $L$  groups, such as  $z_{ik} = 1$  if row  $i$  belongs to row-cluster  $k$  and 0 otherwise (and similarly for  $w_{jl}$ ). Thus, one block is defined by a set of curves which belong to a row and column cluster such as  $z_{ik}w_{jl} = 1$ .

Let us first assume that the partitions  $z$  and  $w$  are independent:

$$p(x; \Theta) = \sum_{z \in Z} \sum_{w \in W} p(z; \Theta)p(w; \Theta)p(x|z, w; \Theta) \quad (4)$$

where  $Z$  is the set of all possible rows partitions into  $K$  groups and  $W$  the set of all possible columns partitions into  $L$  groups. Let us introduce  $\alpha_k$  and  $\beta_l$  as the row and column mixing proportions (belonging to  $[0, 1]$  and summing to 1), such that:

$$p(z; \Theta) = \prod_{ik} \alpha_k^{z_{ik}} \text{ and } p(w; \Theta) = \prod_{jl} \beta_l^{w_{jl}}.$$

Let us also assume that, conditionally on  $(z, w)$ , the curves  $x_{ij}$  are independent and generated by a block-specific distribution:

$$p(x|z, w; \Theta) = \prod_{ijkl} p(x_{ij}; \Theta_{kl})^{z_{ik}w_{jl}}. \quad (5)$$

Unfortunately, the notion of probability density for functional variable is not well defined. In Delaigle and Hall (2010), it is proved that it can be approximated with the probability density of the functional principal components scores (FPCA, Ramsay and Silverman (2005)). Under the assumption (2) of basis expansion decomposition, these FPCA scores are obtained directly from a PCA of the

coefficient  $c$  using a metric defined by the scalar product between the basis function  $\Phi$ . Consequently, model-based approaches for functional data consider probabilistic distribution for either the FPCA scores (Jacques and Preda, 2013, 2014b) or the basis expansion coefficients (Bouveyron et al., 2015, 2020), but it is equivalent.

In addition, depending on the application, the period of observation  $[0, T]$  can be long, and the number of basis functions used for reconstruction can be large. Consequently, the coefficient vectors  $c_{ij}$  may live in high dimensions. In order to suggest a parsimonious data modeling and to avoid the curse of the dimensionality, we further suppose that the curves of each block  $(k, l)$ , for  $k = 1, \dots, K$  and  $l = 1, \dots, L$ , can be described into a low-dimensional functional latent subspace specific to each block, with intrinsic dimension  $d_{kl} < M = S \times R$ . As it will be demonstrated below, this low-dimensional description can be obtained through a principal component analysis for multivariate functional data (MFPCA, Jacques and Preda, 2014b) performed per block. MFPCA is an extension of FPCA to the multivariate functional case, which represents the multivariate curves by a vector of principal scores into an eigenspace formed by multivariate eigenfunctions.

Thus, conditionally to its belonging to block  $(k, l)$ , each multivariate curve  $x_{ij}$  can be represented by its latent counterpart  $\delta_{ij} \in \mathbb{R}^{d_{kl}}$ . Let us define  $Q_{kl}$  the orthogonal matrix of dimension  $M \times M$ , that can be split into two parts:  $Q_{kl} = [U_{kl}, V_{kl}]$  with  $U_{kl}$  of dimension  $M \times d_{kl}$  and  $V_{kl}$  of dimension  $M \times (M - d_{kl})$ . With these notations, the linear mapping from the original space of  $c_{ij}$  to the low-dimensional functional subspace can be written:

$$c_{ij} = \Phi^{-1/2} U_{kl} \delta_{ij} + \epsilon_{ij}.$$

Let us recall that depending on the basis function choice, the orthonormalization matrix  $\Phi$  may be equal to  $I$  (Fourier basis) or not (B-splines, polynomial functions).

Conditionally to the blocks, the latent representations are further assumed to follow a Gaussian distribution with a parsimonious parametrization of the covariance matrix:

$$\delta_{ij} | z_{ik} w_{jl} = 1 \sim \mathcal{N}(m_{kl}, \Delta_{kl}), \quad (6)$$

with  $m_{kl} \in \mathbb{R}^{d_{kl}}$  and  $\Delta_{kl} = \text{diag}(a_{kl1}, \dots, a_{kl d_{kl}})$ . Additionally,  $\epsilon_{ij}$  is assumed to have a centred Gaussian distribution:

$$\epsilon_{ij} | z_{ik} w_{jl} = 1 \sim \mathcal{N}(0, \Xi_{kl})$$

These assumptions induce a Gaussian distribution for the basis expansion coefficients:

$$c_{ij} | z_{ik} w_{jl} = 1 \sim \mathcal{N}(\mu_{kl}, \Sigma_{kl})$$

where  $\mu_{kl} = \Phi^{-1/2} U_{kl} m_{kl}$  and  $\Sigma_{kl} = \Phi^{-1/2} U_{kl} \Delta_{kl} U_{kl}^t \Phi^{-1/2} + \Xi_{kl}$ . Finally,  $\Xi_{kl}$  is assumed to be such

$$Q_{kl}^t \Phi^{1/2} \Sigma_{kl} \Phi^{1/2} Q_{kl} = \left( \begin{array}{c|c} \boxed{\begin{matrix} a_{kl1} & & 0 \\ & \ddots & \\ 0 & & a_{kl d_{kl}} \end{matrix}} & \mathbf{0} \\ \hline \mathbf{0} & \boxed{\begin{matrix} b_{kl} & & 0 \\ & \ddots & \\ 0 & & b_{kl} \end{matrix}} \end{array} \right) \left. \begin{array}{l} \} \\ \} \end{array} \right\} \begin{array}{l} d_{kl} \\ M - d_{kl} \end{array}$$

where  $a_{kl1} > \dots > a_{kl d_{kl}} > b_{kl}$ . With this assumption, the first  $d_{kl}$  values express the main part of the variability of the data, while the remaining ones reflect the variance of the noise and are modeled by a unique parameter  $b_{kl}$ . Thus, the space spanned by the columns of  $U_{kl}$  is a low-dimensional space which contains the main part of information about the data of the block  $(k, l)$ . The remaining information is considered as noise and modeled by a unique variance parameters  $b_{kl}$  for the block  $(k, l)$ .

Thus,  $p(x_{ij}; \Theta_{kl})$  in Eq.(5) can be approximated by  $p(c_{ij}; \mu_{kl}, a_{kl}, b_{kl}, Q_{kl})$ . Let us finally introduce  $\theta_{kl} = (\mu_{kl}, a_{kl}, b_{kl}, Q_{kl})$ . The whole set of model parameters is finally denoted by  $\theta = (\alpha_k, \beta_l, \theta_{kl})_{1 \leq k \leq K, 1 \leq l \leq L}$ .

## 2.3 A family of parsimonious models

In order to provide more parsimonious models, additional assumptions can be made on the different parameters  $a_{kl}$ ,  $b_{kl}$  and  $d_{kl}$ , considering that they are common between clusters or dimensions. This approach allows to generate a family of sub-models of the general model introduced above. In this paper, we will detail the inference procedure to the sub-model assuming  $a_{klm} = a_{kl}, \forall m = 1, \dots, d_{kl}$ , since a good behavior has been observed in practice. Nevertheless, the co-clustering method presented here can be derived for all models of the family extension, following the approach detailed in Bouveyron et al. (2020).

## 3 Model inference

This section focuses on model inference *via* a SEM-Gibbs algorithm. Model selection and initialization will be also discussed.

### 3.1 Model inference through a SEM-Gibbs algorithm

Since we consider the task of co-clustering, the goal is to estimate the unknown row and column partitions  $z_{ik}$  and  $w_{jl}$  given the data at hand. Usually in mixture model, the maximum a posteriori rule is used, based on the estimation of model parameter  $\theta$  maximizing the observed log-likelihood  $L(c; \theta) = \log p(c; \theta)$ .

Unfortunately, the fact that LBM implies a missing structure ( $z$  and  $w$ ) makes the inference harder than in a classical mixture model. Indeed, the maximization of the log-likelihood is not tractable in practice and we have to rely on an iterative inference algorithm.

In such a case where latent variables are involved, one would instinctively use the expectation-maximization (EM) algorithm (Dempster et al., 1977) to find a candidate  $\hat{\theta}$  for the maximum of the log-likelihood. The EM algorithm alternates two steps, the E and M steps, in order to create a converging series of  $\theta^{(h)}$  by optimizing a lower bound of the log-likelihood.

This lower bound can be easily exhibited by rewriting the log-likelihood function as follows:

$$\log(p(c|\theta)) = \mathcal{L}(q(z, w); \theta) + KL(q(z, w) || p(z, w|c, \theta)),$$

where  $\mathcal{L}(q(z, w); \theta) = \sum_{z, w} q(z, w) \log(p(c, z, w, \theta)/q(z, w))$  is a lower bound of the log-likelihood and  $KL(q(z, w) || p(z, w|c, \theta)) = -\sum_{z, w} q(z, w) \log(p(z, w|c, \theta)/q(z, w))$  is the Kullback-Leibler divergence between  $q(z, w)$  and  $p(z, w|c, \theta)$ .

The E step of the EM algorithm consists in maximizing the lower bound  $\mathcal{L}$  over  $q$  for a given value of  $\theta$ . A straightforward calculation shows that  $\mathcal{L}$  is maximized for  $q^*(z, w) = p(z, w|c, \theta)$ . Unfortunately, in our case, the joint posterior distribution  $p(z, w|c, \theta)$  is not tractable as well.

In order to overcome this additional issue, we propose to make use of a Gibbs sampler within the E step to approximate the posterior distribution  $p(z, w|c, \theta)$ . We refer to Keribin et al. (2010) for a discussion on the inference algorithms in the case of latent block models. The resulting stochastic version of the EM algorithm, called SEM-Gibbs hereafter, has the following structure (at iteration  $h$  and starting from an initial column partition  $w^{(0)}$  and initial parameter value  $\theta^{(0)}$ ):

- SE step:  $\theta$  is fixed and  $q^*(z, w) \simeq p(z, w|c, \theta)$  is approximated with a Gibbs sampler. The Gibbs sampler consists in alternating the two following steps a certain number of times to simulate the unknown labels with their conditional distribution knowing the observations and a current estimation of the parameters:

- simulate  $z^{(h+1)} | c, w^{(h)}$  according to:

$$p(z_{ik} = 1 | c, w^{(h)}; \theta^{(h)}) = \frac{\alpha_k^{(h)} f_k(c_i | w^{(h)}; \theta^{(h)})}{\sum_{k'} \alpha_{k'}^{(h)} f_{k'}(c_i | w^{(h)}; \theta^{(h)})}$$

$$\text{with } f_k(c_i | w^{(h)}; \theta^{(h)}) = \prod_{jl} p(c_{ij}; \theta_{kl}^{(h)}) w_{jl}^{(h)}.$$

– simulate  $w^{(h+1)}|c, z^{(h+1)}$  according to:

$$p(w_{jl} = 1|c, z^{(h+1)}; \theta^{(h)}) = \frac{\beta_l^{(h)} f_l(c_j|z^{(h+1)}; \theta^{(h)})}{\sum_{l'} \beta_{l'}^{(h)} f_{l'}(c_j|z^{(h+1)}; \theta^{(h)})}$$

$$\text{with } f_l(c_j|z^{(h+1)}; \theta^{(h)}) = \prod_{ik} p(c_{ij}; \theta_{kl}^{(h)})^{z_{ik}^{(h)}}.$$

• M step:  $\mathcal{L}(q^*(z, w), \theta^{old})$  is now maximized over  $\theta$ , where :

$$\begin{aligned} \mathcal{L}(q^*(z, w), \theta^{old}) &\simeq \sum_{z, w} p(z, w|c, \theta^{old}) \log(p(c, z, w|\theta)/p(z, w|c, \theta^{old})) \\ &\simeq E[\log(p(c, z^{(h+1)}, w^{(h+1)}|\theta)|\theta^{old})] + \xi, \end{aligned}$$

$\xi$  being a constant term regarding  $\theta$ . This step therefore reduces to the maximization of the conditional expectation of the complete-data log-likelihood given  $c$ ,  $z^{(h+1)}$  and  $w^{(h+1)}$  (Appendix A.1 provides a developed form of  $E[\log(p(c, z^{(h+1)}, w^{(h+1)}|\theta)|\theta^{old})]$  and conduces to the following updates for model parameters.

The mixing proportion and the block mean are updated as follows:

$$\begin{aligned} - \alpha_k^{(h+1)} &= \frac{1}{n} \sum_i z_{ik}^{(h+1)} \text{ and } \beta_l^{(h+1)} = \frac{1}{p} \sum_j w_{jl}^{(h+1)}, \\ - \mu_{kl}^{(h+1)} &= \frac{1}{n_{kl}^{(h+1)}} \sum_{ij} z_{ik}^{(h+1)} w_{jl}^{(h+1)} c_{ij} \text{ with } n_{kl}^{(h+1)} = \sum_{ij} z_{ik}^{(h+1)} w_{jl}^{(h+1)}. \end{aligned}$$

For the variance parameters  $a_{kl}$ ,  $b_{kl}$  and  $Q_{kl}$ , let us define the sample covariance matrix  $\Omega_{kl}^{(h)}$  of block  $kl$  at step  $h$ :

$$\Omega_{kl}^{(h)} = \frac{1}{n_{kl}^{(h)}} \sum_{i=1}^n \sum_{j=1}^M z_{ik}^{(h+1)} w_{jl}^{(h+1)} (c_{ij} - \mu_{kl}^{(h)})^t (c_{ij} - \mu_{kl}^{(h)}).$$

Then, the updates for  $a_{kl}$ ,  $b_{kl}$  and  $Q_{kl}$  are:

- the variance parameters  $a_{kl}^{(h+1)}$ , are updated by the mean of the  $d_{kl}$  largest eigenvalues of  $\Phi^{1/2} \Omega_{kl}^{(h)} \Phi^{1/2}$ ,
- the variance parameters  $b_{kl}$  are updated by  $\frac{1}{M-d_{kl}} (\text{trace}(\Phi^{1/2} \Omega_{kl}^{(h)} \Phi^{1/2}) - d_{kl} a_{kl}^{(h)})$ ,
- the  $d_{kl}$  first columns of the matrix of eigen functions coefficients  $Q_{kl}^{(h)}$  are updated by the eigen functions coefficients associated with the largest eigenvalues of  $\Phi^{1/2} \Omega_{kl}^{(h)} \Phi^{1/2}$ .

Proofs of those results are available in Appendices A.2, A.3 and A.4.

## 3.2 Algorithmic considerations

**Implementation** Regarding the practical implementation, the SEM-Gibbs algorithm is run for a given number of iterations. After a burn-in period, the final estimation  $\hat{\theta}$  of the parameters is obtained by the mean of the sample distribution (without the burn-in iterations). Then, a new Gibbs sampler is used to sample  $(\hat{z}, \hat{w})$  according to  $\hat{\theta}$ , and the final partition  $(\hat{z}, \hat{w})$  is obtained by the marginal mode of this sample distribution.

**Initialization of the algorithm** As said previously, our algorithm relies on a SEM-Gibbs algorithm. This algorithm needs to be initialized carefully with values for column partitions and parameters, or similarly with both column and row partitions. To this end, we consider the three following initialization strategies: *random*, *k-means* and *funFEM*. In the *random* case, row and column partitions are randomly sampled from a multinomial distribution with uniform probabilities. The *k-means* strategy consists in initializing the two partitions with those obtained by *k-means* directly applied on a discretized version of the data matrix and its transpose. Finally, the *funFEM* strategy initializes the partitions by applying the *funFEM* algorithm (Bouveyron et al., 2015) on the matrix concatenating the functional variables and its transpose. We will see later, in the numerical experimentation section, that *funFEM* is the one that gives the best results.

### 3.3 Choice of the number of clusters

We now discuss the choice of the hyper-parameters  $K$  and  $L$ , *i.e.* the number of row clusters and column clusters respectively. The choice of these hyper-parameters is viewed here as a model selection problem. Well established model selection tools are Akaike information criterion (AIC, Akaike 1974), Bayesian information criterion (BIC, Schwarz 1978) and Integrated Classification Likelihood (ICL, Biernacki et al. 2000). However, in the co-clustering case, the likelihood is not tractable for the same reason than the EM algorithm is not usable. Consequently, AIC and BIC are not tractable. Conversely, the ICL criterion can still be considered since it relies on the completed data log-likelihood, which is tractable. Adapted to our model, the ICL criterion is:

$$ICL(K, L) = \log p(c, \hat{z}, \hat{w}; \hat{\theta}) - \frac{K-1}{2} \log(n) - \frac{L-1}{2} \log(p) - \frac{\nu}{2} \log(np)$$

where  $\nu = KLM + 2KL + \sum_{kl} d_{kl}(M - \frac{d_{kl}+1}{2})$  is the number of continuous parameters per block and

$$\log p(c, \hat{z}, \hat{w}; \hat{\theta}) = \prod_{ik} \hat{z}_{ik} \log(\alpha_k) + \prod_{jl} \hat{w}_{jl} \log(\beta_l) + \sum_{ijkl} \hat{z}_{ik} \hat{w}_{jl} \log p(c_{ij}; \hat{\theta}_{kl}).$$

The couple  $(K^*, L^*)$  leading to the highest ICL value is selected as the most appropriate number of row and column clusters.

## 4 Numerical experimentation on simulated data

This section presents numerical experiments on simulated data in order to illustrate the behavior of the proposed methodology in presence of different noise ratio in data and to study the selection of the number of row and column clusters. The R code for our multivariate functional co-clustering algorithm is currently available under request and will be soon available on CRAN as an R package.

### 4.1 Simulation setup

We first detail here the simulation setup that is used in the following numerical experiments. Bivariate curves ( $S = 2$ ) are simulated with  $K = 4$ ,  $L = 3$ . The proportions of row clusters  $\alpha$  used is  $(0.2, 0.4, 0.1, 0.3)$  and column clusters  $\beta$  is  $(0.4, 0.3, 0.3)$ . The first functional variable is designed from four different functions that are used as blocks mean at 31 equi-spaced time points,  $t = 0, 1/30, 2/30, \dots, 1$ :

$$x_{ij}(t) | z_{ik} w_{jl} = 1 \sim \mathcal{N}(m_{kl}(t), s^2),$$

where  $s = 0.3$ . The block mean functions  $m_{kl}$  are such that  $m_{11} = m_{21} = m_{33} = m_{42} = f_1$ ,  $m_{12} = m_{22} = m_{31} = f_2$ ,  $m_{13} = m_{32} = f_3$  and  $m_{23} = m_{41} = m_{43} = f_4$ , with  $f_1(t) = \sin(4\pi t)$ ,  $f_2(t) = 0.75 - 0.5 \mathbb{1}_{t \in ]0.7, 0.9[}$ ,  $f_3(t) = h(t)/\max(h(t))$  where  $h(t) = \mathcal{N}(0.2, \sqrt{0.02})$  and  $f_4(t) = \sin(10\pi t)$ . Then the second variable is designed according to the same process than the first one but with four different functions:  $f_1(t) = \cos(4\pi t)$ ,  $f_2(t) = 0.75 - 0.5 \mathbb{1}_{t \in ]0.2, 0.4[}$ ,  $f_3(t) = h(t)/\max(h(t))$  where  $h(t) = \mathcal{N}(0.2, \sqrt{0.05})$  and  $f_4(t) = \cos(10\pi t)$ . The block means functions of the two functional variables are shown on Figure 4.

Starting from this simulation setting, five scenarios are derived by adding some noise fraction within the blocks by randomly simulating a percentage  $\tau$  of curves using other block means: 0% (scenario 1), 10% (scenario 2), 30% (scenario 3), 50% (scenario 4) and 80% (scenario 5).

Regarding the algorithm setup, we set to 50 iterations the burn-in period of the algorithm and the SEM-Gibbs maximal number of iterations is set to 100.

### 4.2 Robustness to noise and influence of initialization

This first experiments aims at studying the ability of our algorithm to recover the simulated model in clean but also noisy situations, and depending on the type of initialization of the SEM-Gibbs



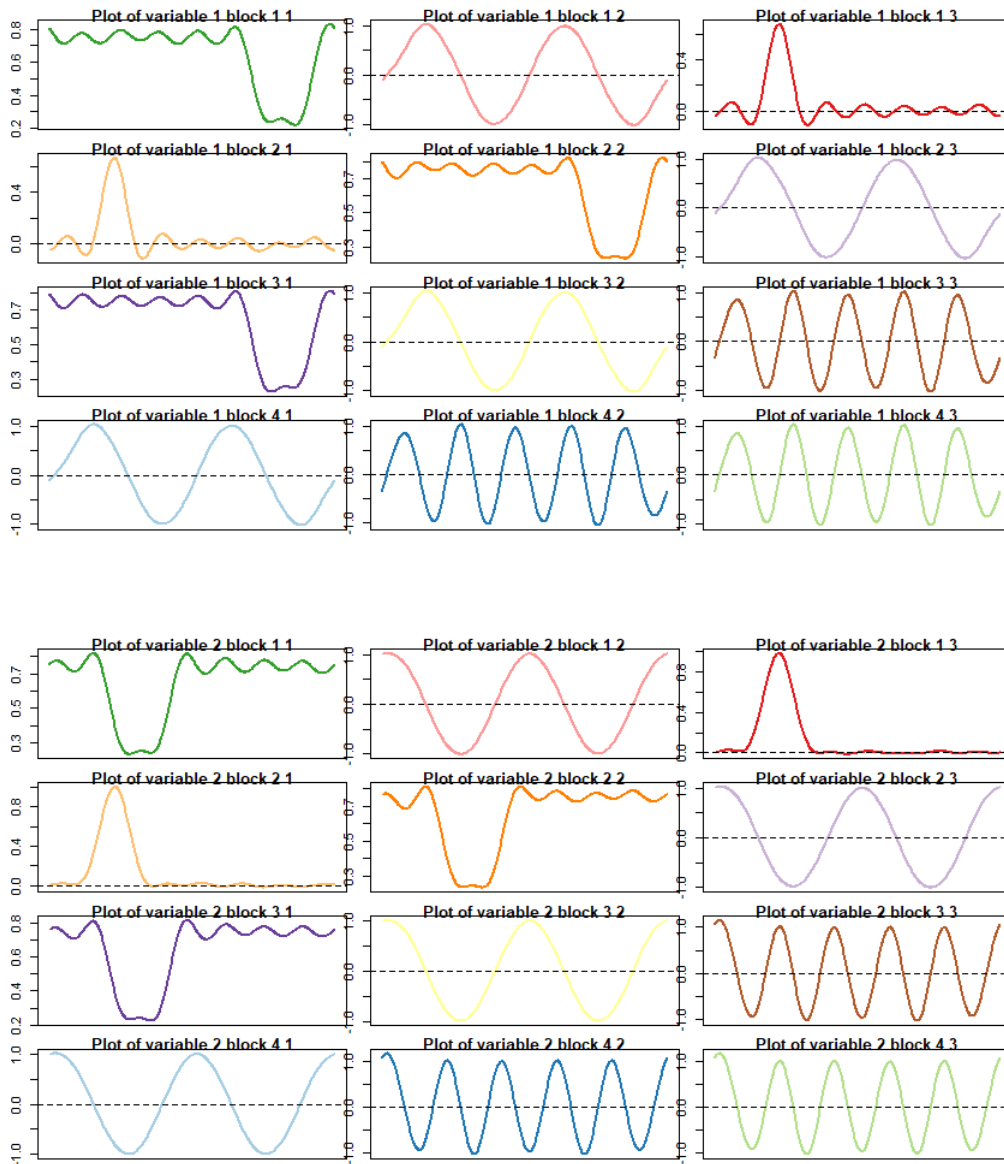


Figure 4: Block means functions for the first variable (top) and second variable (bottom)

algorithm. To this end, 20 simulations with  $n = p = 100$  have been performed for each scenario with both *k-means*, *funFEM* and *random* initializations. The algorithm is applied for  $K = 4$  and  $L = 3$  and with Fourier smoothing with 15 basis functions. The quality of estimated partitions is assessed with the Adjusted Rand Index (ARI, Rand 1971). We recall that an ARI of 1 indicates that the partition provided by the algorithm is perfectly aligned with the simulated one. Conversely, an ARI of 0 indicates that the two partitions have just some random matches.

Results are shown in Figure 5 for both row (left panels) and columns partitions (right panels). We can see that co-clustering results are almost perfect for the 4 first scenarios with *funFEM* initialization (bottom panels), and the 2 first scenarios for *k-means* initialization. As expected, the algorithm performance decreases while noise increases, but median ARI value is always above 0.8 in the case of four first scenarios with *k-means* and *funFEM* initialization. Moreover *k-means* initialization performs better than random when the noise ratio is upper than 50%. And the *funFEM* initialization performs better than the *k-means* one. In view of the good behaviour of *funFEM* initialization, we recommend to use the *funFEM* initialization rather than the two others available in the algorithm.

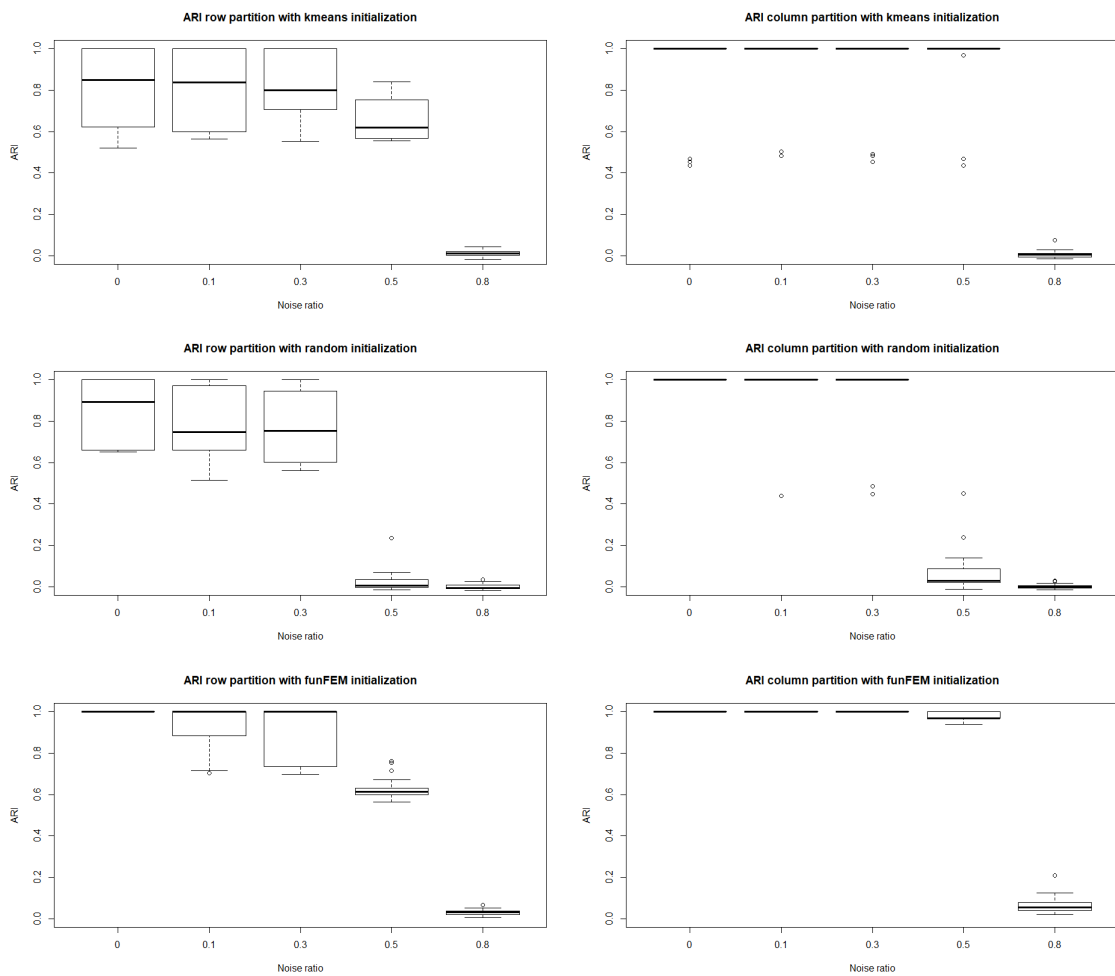


Figure 5: ARI results for our SEM-Gibbs according to the noise ratio and depending on the type of initialization: *k-means* (top), random (middle) and *funFEM* (bottom).

### 4.3 Model selection

In this section, the selection of the number of clusters using the ICL criterion we derived earlier is investigated. Data are generated as previously. The simulation setting is repeated 20 times with  $n = 500$ ,  $p = 500$  and  $T = 30$ . For each of the 20 generated data sets, the SEM-Gibbs algorithm

is run with  $K$  and  $L$  values ranging from 2 to 6 clusters, with *funFEM* initialization. Each time, the model selected by ICL is reported. Results are shown in Table 1. The results indicate that our SEM-Giibs algorithm in combination with the ICL criterions is able to perfectly recover the actual model with a noise ratio from 0 to 30% of the data volume. Then, as expected, the performance of the criterion decreases. For a noise ratio of 50%, the ICL criterion is however still able to identify the actual simulation model in 90% of the cases. Finally, for 80% of noise, the algorithm not being able to recover the partitions (Figure 5), the ICL criterion is also not able to find the number of co-clusters.

Table 1: Percentage of selection of each model  $(K, L)$  by ICL among the 20 simulated data sets. The actual values for  $(K, L)$  are  $(4, 3)$ .

Scenario $\tau = 0$						Scenario $\tau = 0.3$						Scenario $\tau = 0.5$					
$K/L$	2	3	4	5	6	$K/L$	2	3	4	5	6	$K/L$	2	3	4	5	6
2	0	0	0	0	0	2	0	0	0	0	0	2	0	0	0	0	0
3	0	0	0	0	0	3	0	0	0	0	0	3	0	0	0	0	0
4	0	<b>100</b>	0	0	0	4	0	<b>100</b>	0	0	0	4	0	<b>90</b>	0	0	0
5	0	0	0	0	0	5	0	0	0	0	0	5	0	10	0	0	0
6	0	0	0	0	0	6	0	0	0	0	0	6	0	0	0	0	0

## 5 Co-clustering of environmental data from Région Sud

### 5.1 Data and pretreatments

The environmental database is composed by five variables, namely three pollutants (maximum of  $\text{NO}_2$  and  $\text{O}_3$  and average of  $\text{PM}_{10}$ ) and two meteorological measurements (average of temperature (T) and pressure (P)). On the spatial point of view, the measurements are collected on a resolution of 4 km: the region is divided in 4km squares, each square represent a measure, constituting a mesh of 1995 and 1967 for pollution and meteorological variables respectively (Figure 6A-B). Unfortunately, the two meshes do not overlap, thus we needed to set up a procedure to reconcile the two databases.

It was first necessary to manage the missing data from the weather and pollution databases: there were 2 % of days missing for the pollution data and 1 % for the weather data over 2191 days between 2013 and 2018. Out of scale measurements due to captures failures or modeling errors were identified and considered and treated as missing data. When data are missing, no square of the mesh has a value associated, thus we need to reconstruct the data for the entire region over the days that are missing. Two methods were used: interpolation and random sampling. The interpolation method was used for variables with a periodic trend or a seasonality ( $\text{PM}_{10}$ ,  $\text{O}_3$ , P, T) whereas the random sampling method was considered for other variables ( $\text{NO}_2$ ). The interpolation method was done with the `na.approx()` function of the R package "zoo". Regarding the random sampling method, the values that replace the missing data are taken from a window of variable size around the missing data period. The window size adapts according to the period (i.e. day/s) of missing data to replace: specifically it is equivalent to 4 days + the length of the missing period divided by 2.

In order to reconcile the pollution and meteorological databases constituted on the two different meshes and to make data easier to interpret, we decided to change the data resolution, specifically we created 357 zones (Figure 6C). These zones represent non-overlapping postal codes. A postal code can be associated with several municipalities but can also be different for the same municipality (4 postal codes in Nice for example). Environmental data therefore had to be transformed from the 4 squares km to the zone level. The association was therefore made in 2 stages, firstly an association of pollution data - zones then weather data - zones and finally pollution-weather data at zone level. Briefly, when a 4 km square covers the largest area of a zone, it is associated with it. Thus we ended up with an environment database of 357 lines, corresponding to the zones of the region, for each pollution and weather variable. The pollution and meteorological data associated to each zone, represent the maximal or the average value of the squares included in the zone. Accordingly, if a zone

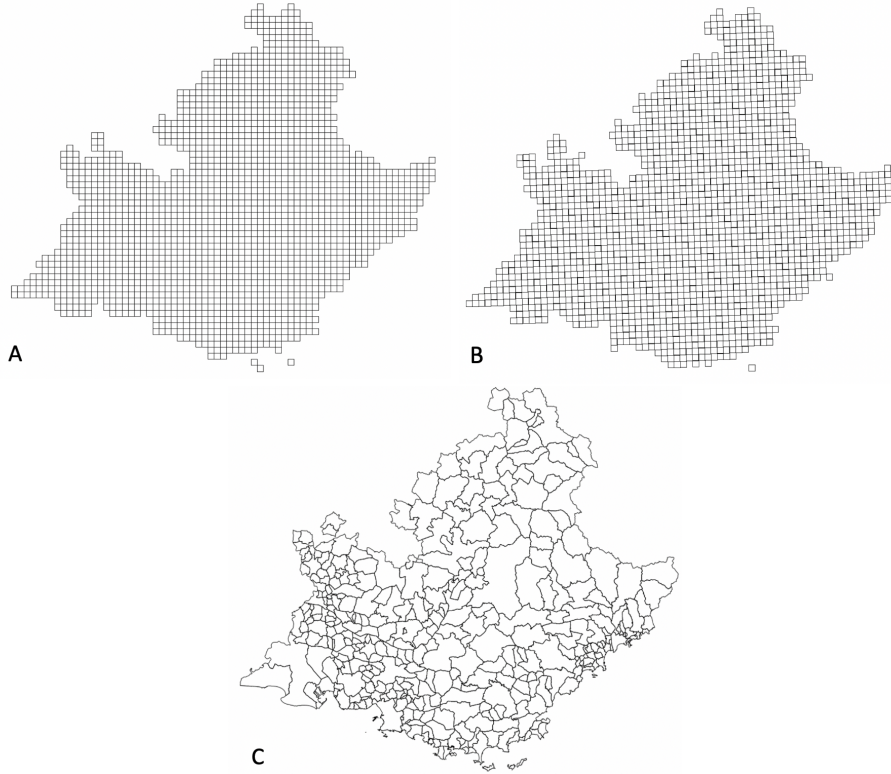


Figure 6: Non-overlapping meshes of squares of 4 km for pollution (A) and meteorological (B) data. (C) Région Sud divided in 357 zones of non-overlapping postal codes.

cover only one square, it will assume the values associated to the single square. We chose the maximal value for  $\text{NO}_2$ ,  $\text{O}_3$  and the average value for  $\text{PM}_{10}$ , T and P to respect the original measurement done at the mesh level.

## 5.2 Experimental protocol

In order to test the ability of multiFunLBM to identify spatio-temporal profiles, we used daily measurements of our five variables, in the 357 zones of the Région Sud, for a period of six years from 2013 to 2018 for a total of 2191 measurements per variable per zone. Firstly, the variables were standardized in order to be compared easily. They were also transformed into functional data by weeks (7 days, start from Tuesday) using a Fourier basis. We chose the week as the time window, because we needed a window to divided evenly the period under investigation. There are exactly 313 weeks of 7 days in the period concerned by the study. The Fourier basis was chosen for reconstructing the functions because some variables exhibit a clear periodicity. The number of basis function was set to 7. Then, the multiFunLBM algorithm was applied to the environmental database. The number of clusters on the spatial and temporal dimensions (respectively,  $K$  and  $L$ ) were allowed to vary in the range 2 to 10. The appropriate number of clusters was assessed according to ICL criterion (maximum) and the type of initialization used was *funFEM*.

## 5.3 Results

The algorithm identified  $K = 6$  clusters for the spatial dimension, and also  $L = 6$  clusters for the temporal dimension (see Figures 7A and 7B respectively). Figure 7A shows the frequency and the number of zones (postal codes) in each cluster. The spatial distribution of the six clusters is shown in Figure 8. Overall, the clusters well represent the different zones of the region: cluster 3 groups all zones in the mountains, cluster 6 represents the west part of the region, which is organized along

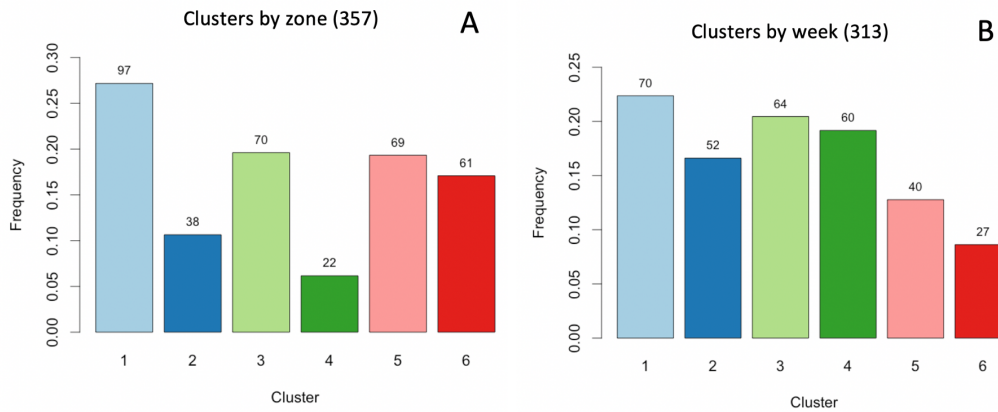


Figure 7: Frequency of the 6 clusters identified by multiFunLBM on the spatial (A) and temporal (B) dimension, respectively. The number of zones (A) or weeks (B) for each cluster is reported.

the Rhône river. The zones on the coast are divided in two clusters : cluster 4 that groups the most populated and industrialized zones of the region including the city of Marseille and Nice, while cluster 2 collects the others. Interestingly, all zones where the main highway of the region pass by are clustered in cluster 5. Finally, rural zones with are gathered in cluster 1. This segmentation confirms that pollution levels are correlated with the geography and the human activity, and that our clustering approach well identifies intrinsic structures of the territory.

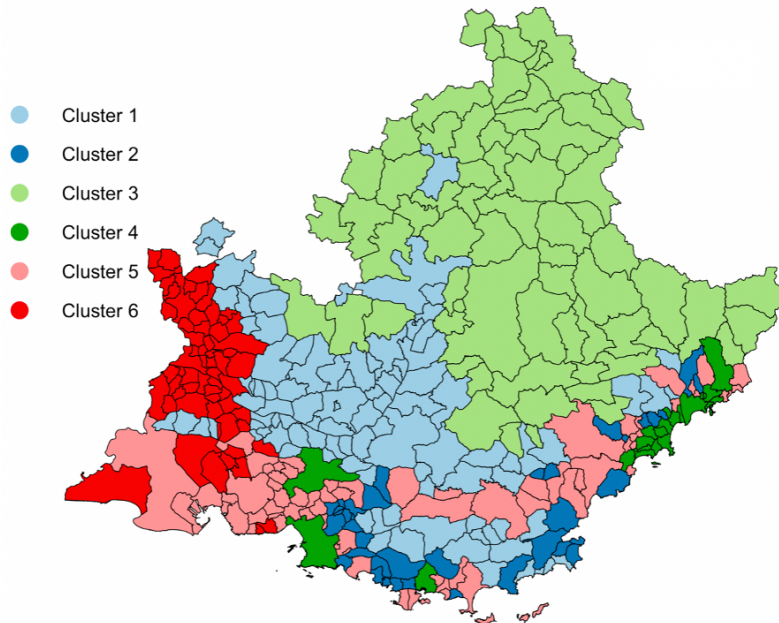


Figure 8: Association of the 357 zones in Région Sud with the clusters on the spatial dimension. Color code is indicated in the figure.

The analysis on the temporal dimension is done by weeks, meaning that the behavior of the five environmental variables is studied with a week resolution. On this dimension, six clusters were identified as well: cluster 1 is the biggest one with 70 weeks (22 %) and cluster 6 the smallest with 27 weeks (9 %), see Figure 7B. Tables 2–4 in Appendix A.5 show respectively the number of weeks by cluster by year, month and season. Figure 9 presents a calendar representation of the 313 weeks by cluster. Interestingly, the clusters mainly group the weeks accordingly to the seasons, independently by

the year, proving the ability of multiFunLBM to find out data structures and the intrinsic link between pollution and meteorological factors due to the seasons. Specifically, cluster 2 mainly collects summer weeks (June, July, August) all over the six years, while cluster 1 and cluster 5 winter and late autumn ones (November, December, January and February). Spring and early autumn (March, April, May, September and October) weeks are in two clusters, cluster 3 and 4. Finally cluster 6 collects sporadic weeks all over the six years regardless the season, suggesting perhaps peculiar pollution trends in these weeks.



Figure 9: Association of the 313 weeks for the period from 2013 and 2018 in Région Sud with the clusters on the temporal dimension. Color code is indicated in the figure.

We hereafter propose a deeper analyses of the results regarding the different functional variables.

### 5.3.1 Meteorological variables

To explore the profiles of the five variables by cluster, we plot the average week profiles for each spatial and temporal cluster obtaining 36 profiles for each variable represented in Figure 10 for meteorological and Figures 11, 12 for pollution variables. Each plot represents the average curve by day of the week of the environmental variable measurements for all the weeks and zones contained in each cluster. For instance, the top-left panel shows for each variable the average week profile for all zones contained in cluster 1 on the spatial dimension (97 zones mainly rural) on the weeks falling in cluster 1 on the temporal dimension (70 weeks, mainly winter and late autumn), and so on for the other plots.

Meteorological variables, especially average of temperatures, show flat profiles within a cluster, meaning that no week trend is observed, as expected (Figure 10). Temperature profiles perfectly reflects what expected by season and zone of the region (refer to Figure 10A): winter weeks grouped



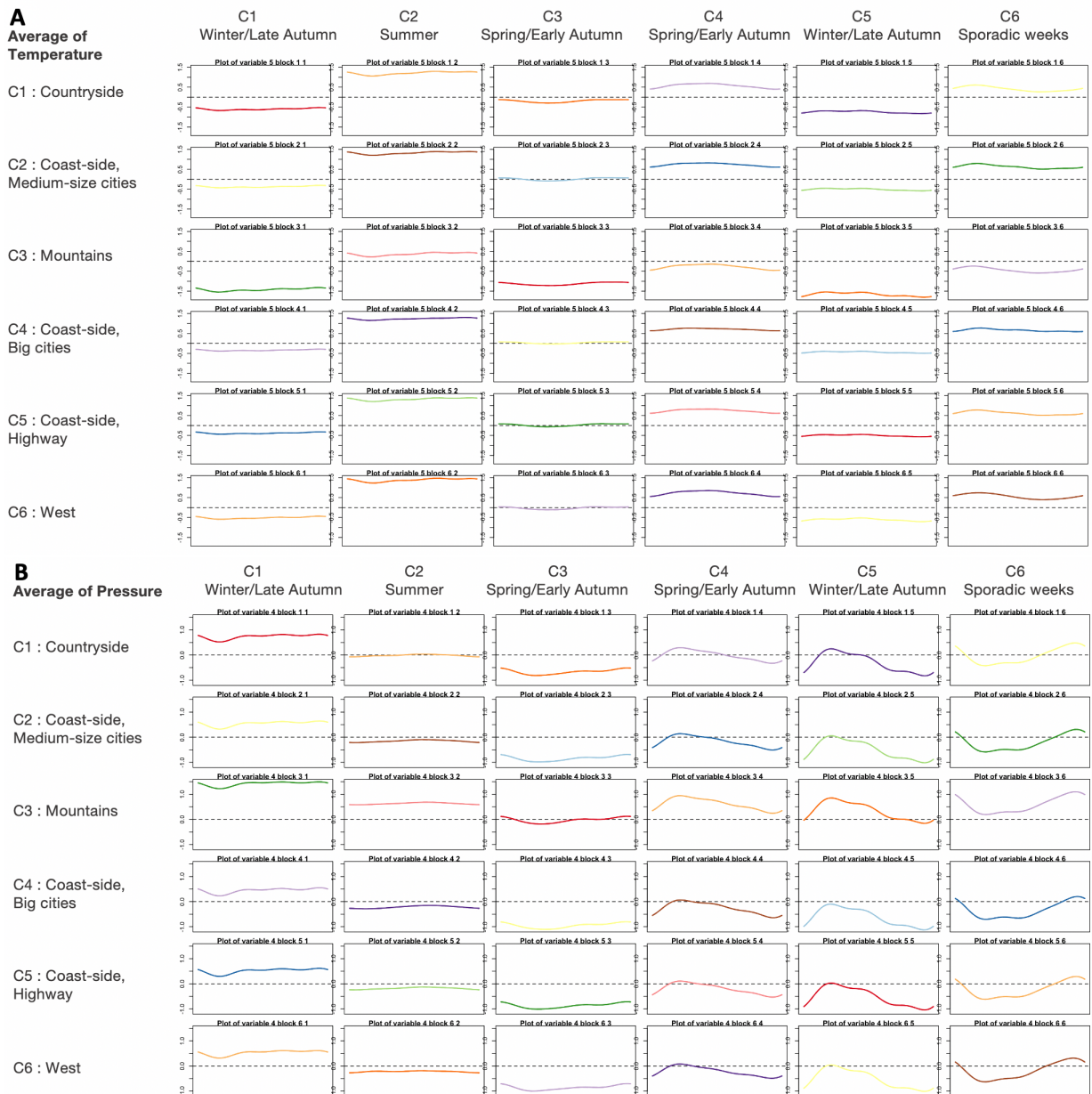


Figure 10: Mean profiles by cluster on temporal (columns) and spatial (rows) dimensions for meteorological variables : temperature (A) and pressure (B).

in clusters 1 and 5 on the temporal dimension (columns) are below the mean level, with the lowest reached for zones on the mountains collected in cluster 3 on the spatial dimension (rows). A similar trend but with opposite values (above the mean) is observed for temporal cluster 2, summer weeks. Conversely, clusters 3 and 4 exhibit quite opposite trends for spring and early autumn weeks, showing the coldest and the warmest profiles respectively, despite the spatial clusters.

Regarding the pressure, expected observations can be done: the highest levels are reached for spatial cluster 3 (mountains) independently by the temporal clusters. On the temporal clusters point of view, the highest levels are obtained for profiles in cluster 1 (winter and late autumn) and the lowest in cluster 3 (spring and early autumn), while summer weeks (cluster 2) show flat profiles around the average. Cluster 4 (spring and early autumn), 5 (winter and late autumn) and 6 (sporadic weeks) on the temporal dimension show profiles modulated by the day of the week, with the highest values in the middle of the week (Wednesday, Thursday and Friday) and the lowest in the week-end plus Monday and Tuesday, for the formers, opposite pattern for the latter.

### 5.3.2 Pollution variables

**Ozone** Pollutant variable profiles mostly vary according to the day of the week. As it can be seen on Figure 11A, the most stable trends on the week window are for maximum of  $O_3$ , due to the strong dependency of this pollutant by the season more than the day of the week. Indeed,  $O_3$  levels depend on heat and sunshine. The seasonality of this pollutant is well identified by multiFunLBM because profiles are similar by column (temporal dimension) and not by row (spatial dimension). The lowest levels are for temporal cluster 1 and 5 (winter and late autumn), while the highest are for cluster 2 (summer) independently of the cluster on the spatial dimension. Interestingly, as observed for meteorological variables, the two clusters of spring and early autumn weeks (cluster 3 and 4), although they collect weeks from the same period of the year, they do not show similar profiles intra-variables, but each cluster have similar trend inter-variable, confirming the strong relationship between  $O_3$  and meteorological factors, mainly temperature. Overall the  $O_3$  seems not to have a strong spatial dependence, since profiles by temporal dimensions looks similar among clusters of the zones of Région Sud. We however observe a strong temporal dependence with the highest levels in summer.

**Particulate matters** Levels of PM10 depend on intensive anthropogenic activities, such as fossil fuel combustion and biomass burning, and thus we expect a strong spatial dependence. Accordingly, multiFunLBM well finds that spatial cluster 5 (zones on the high-way), cluster 4 (big-cities on the coast) and cluster 6 (west), regardless of the temporal clusters, always show the highest levels, as reported in Figure 11B. Interestingly, we found high levels of PM10 in spatial cluster 1 (countryside) probably because of the biomass burning practice due to agricultural and gardening activities that produce high quantities of particles. Overall, higher levels of average of PM10 are observed mainly in wintertime (cluster 1 and 5 on the temporal dimension) due to a higher use of heating systems and fossil fuel combustion than in summer time. Clusters 1, 4, 5 and 6 on the temporal dimension show clearly the weekly dependency of this pollutant, even though with different levels: all these clusters show higher level of PM10 in the middle of the week (Tuesday, Wednesday and Thursday) and lowest in week-ends and Monday, probably suggesting that industrial activities and traffic due to working days have the strongest influence on the concentrations of this pollutant.

**Nitrogen Dioxide** More than 50 % of the  $NO_2$  presents in the air is produced by fuel combustion and cars, and is mainly present in densely populated areas. Thus, as expected, the spatial clusters 4 (big cities on the coast) and 5 (zones on the highway) have high levels of maximum of  $NO_2$  regardless of the season (clusters on temporal dimension), as showed in Figure 12. Temporal clusters 1 (winter and late autumn) and 2 (summer) show very similar profiles and levels on the spatial dimension, demonstrating the high spatial dependence of this pollutant that is not influenced by climatic factors due to seasonality. As observed for the other pollutants, spring and early autumn weeks of the six years under study are grouped in two clusters that show two profiles: cluster 3 has a flat profile, i.e. pollutant concentration does not depend on the day of the week, cluster 4 exhibits high levels during the week with a drop during the week-ends. These two clusters show that pollution concentrations in this time of the year is affected by working activities more than in other periods. Overall,  $NO_2$



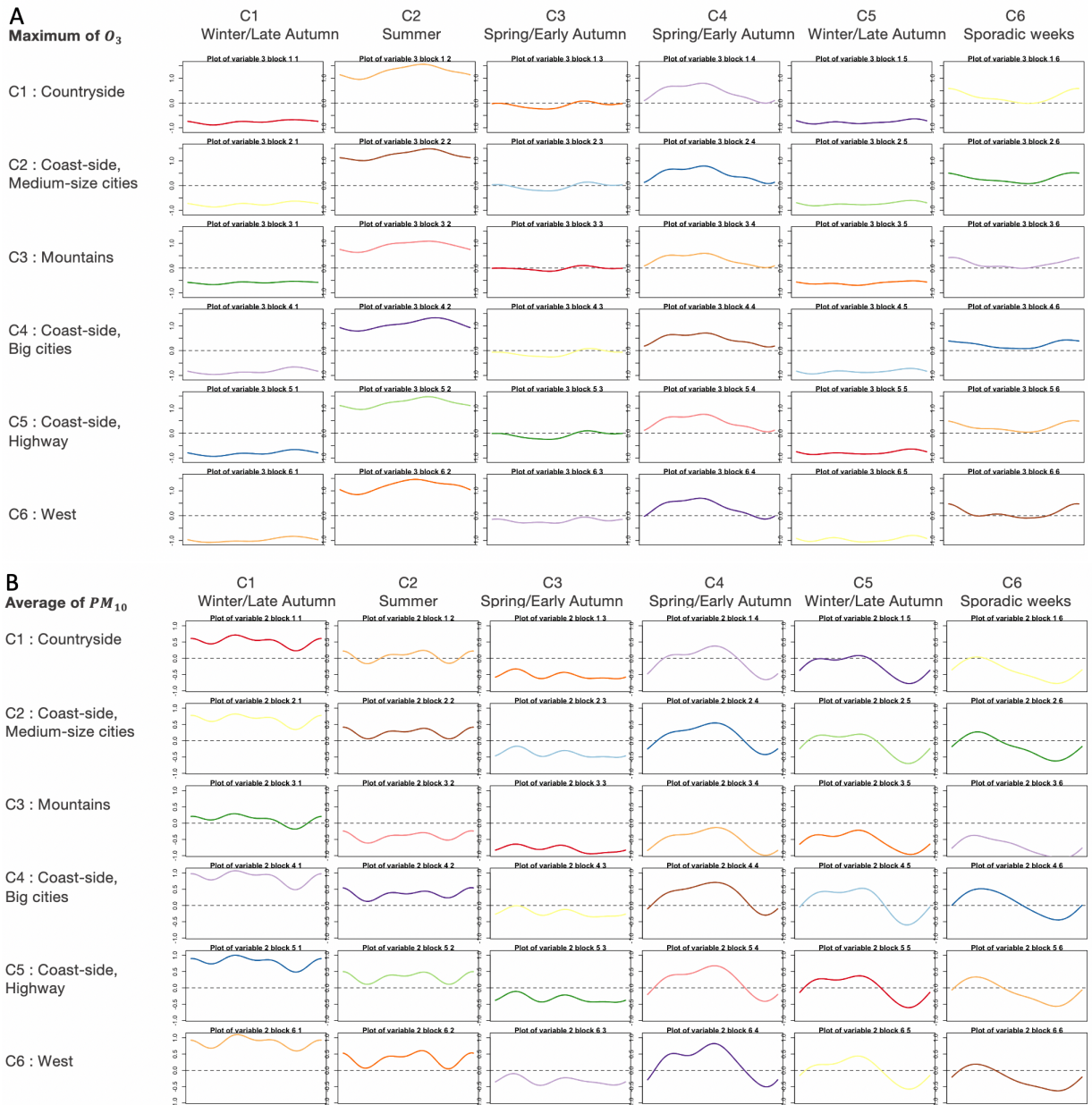


Figure 11: Mean profiles by cluster on temporal (columns) and spatial (rows) dimensions for maximum of  $O_3$  (A) and average of  $PM_{10}$  (B).

shows quite strong week trends, with high levels during the week and low levels in the week-end due to public and private traffic trends accordingly with working days.

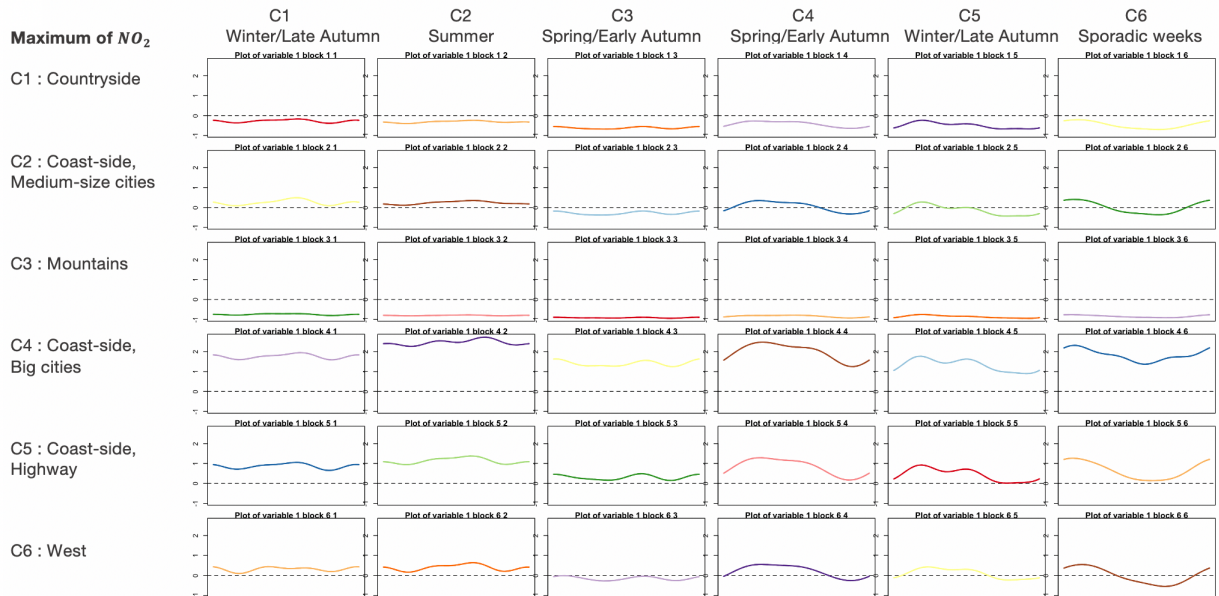


Figure 12: Mean profiles by cluster on temporal (columns) and spatial (rows) dimensions for maximum of  $\text{NO}_2$ .

## 5.4 Summary of the results

The six clusters on the spatial dimension collect zones on the mountains, rural areas, west side of the region. Furthermore, the algorithm differentiates as well zones on the coast line depending on habitant proportions and industrialization levels. Surprisingly it also identified one cluster that collects all the zones where the main highway of the region pass by. On the other dimension, the 313 weeks of the period under investigation are as well collected in clusters respecting the seasonal trends: winter and late autumn, spring and early autumn, summer. Policies against pollution raise are usually taken at the department level (5 in the Région Sud). However a department represents a very heterogeneous territory with different industrialization levels, inhabitant proportions and geographical composition, making hard to find policies that well suit all the diverse scenarios. The clusters identified by multiFunLBM may be used by local authorities in order to set up specific policies to lower down pollution or for public alerts when pollution raise above secure levels for the citizens that adapt to the different areas. Furthermore the temporal clusters can help to spot periods of the years that are particularly affected by pollution at the level of the spatial clusters, in order to set up alerts and prevention behaviors for each specific zone.

## 6 Discussion and conclusion

This work was prompted by the need to analyze air pollution in the South of France in order to help the AtmoSud agency and local institution to monitor pollutants dynamics and to spread public alerts when necessary. Here we introduced a co-clustering of multivariate functional data to fulfill these objectives. The multiFunLBM algorithm allows to cluster both individuals (zones) and columns (weeks) simultaneously, in order to propose a summary of the data through homogenous blocks of functional data. The proposed approach relies on a functional latent block model, which assumes for each block a probabilistic distribution for the scores of the multivariate curves obtained from a multivariate functional principal component analysis. Model inference is based on a SEM-Gibbs

algorithm which alternates a SE-step where row and column partitions are simulated according to Gibbs algorithm, and a M-step where model parameters are updated conditionally on the previous simulated partitions. Model selection relies on the ICL criterion which has been specifically derived for the proposed model. As far as the authors know, this is the first algorithm available for functional multivariate co-clustering.

The multiFunLBM algorithm has been used to analyze an environmental database supplied by the AtmoSud agency, collecting daily measurements of three pollutants along with pressure and temperature for a period of 6 years in the south of France. Without any knowledge about the geographical composition of the territory nor the specific seasonality of the territory, the algorithm identifies fine and meaningful clusters, both on the spatial and temporal dimensions. These clusters could be used in a near future to help local authorities to issue public alerts that are specific to more restricted areas.

On a larger dimension, the understanding of the spatio-temporal dynamic of air pollution is a current challenge world-wide. Several agencies have been created world-wide in order to monitor air pollution behavior, to identify factors influencing pollution peaks before alerting local authorities and citizens. Nevertheless, air pollution dynamic is extremely complicated and affected by many factors including meteorological variables such as temperature, pressure, wind speed, rain, humidity etc. Due to the high amount of variable to take into account, there is the tendency to focus pollution studies behavior only on big cities, as the main producers of pollution. However mass of air moves over bigger territories than single cities, thus spreading the pollution to adjacent areas. There is therefore a need to analyse air pollution on large territories, taking into account not only pollutants but also meteorological factors, and we believe that tools such that multiFunLBM may be useful in such a context.

**Acknowledgements** The authors would like to specially thank the AtmoSud institute (<http://atmosud.org>) for providing the data. This research has benefited from the support of the "FMJH Research Initiative Data Science for Industry". This work has also been supported by the French government, through the 3IA Côte d'Azur and UCAJEDI Investments in the Future project managed by the National Research Agency (ANR) with the reference numbers ANR-19-P3IA-0002 and ANR-15-IDEX-01.

## A Appendix

### A.1 Developed form of $E[\log(p(c, z^{(h+1)}, w^{(h+1)}|\theta)|\theta^{old})]$

The conditional expectation of the complete-data log-likelihood  $H(\theta|\theta^{old})$  has the following form for the model proposed in this work:

$$\begin{aligned} H(\theta|\theta^{old}) &= E[\log(p(c, z^{(h+1)}, w^{(h+1)}|\theta)|\theta^{old})] \\ &= \sum_{i,k} z_{ik}^{(h+1)} \log \alpha_k + \sum_{j,l} w_{jl}^{(h+1)} \log \beta_l + \sum_{i,j,k,l} z_{ik}^{(h+1)} w_{jl}^{(h+1)} \log(p(c_{ij}; \theta_{kl})), \end{aligned} \quad (7)$$

where  $z_{ik}^{(h+1)} = E[z_{ik}|\theta^{old}]$  and  $w_{jl}^{(h+1)} = E[w_{jl}|\theta^{old}]$ . In order to ease the reading of the reminder, the subscript  $^{(h+1)}$  will be omitted hereafter. Let us now focus on the last quantity of the previous equation.

$$\sum_{i,j,k,l} z_{ik} w_{jl} \log(p(c_{ij}; \theta_{kl})) = \sum_{i,j,k,l} z_{ik} w_{jl} \log\left(\frac{1}{(2\pi)^{M/2}} |\Sigma_{kl}|^{-1/2} \exp\left(-\frac{1}{2}(c_{ij} - \mu_{kl})^t \Sigma_{kl}^{-1} (c_{ij} - \mu_{kl})\right)\right),$$

where  $\Sigma_{kl} = \Phi^{-1/2} Q_{kl} \Delta_{kl} Q_{kl}^t \Phi^{-1/2} + \Xi_{kl}$ . Let  $n_{kl} = \sum_{i=1}^n \sum_{j=1}^M z_{ik} w_{jl}$  be the number of curves belonging to the block  $(kl)$ , then:

$$\begin{aligned} \sum_{i,j,k,l} z_{ik} w_{jl} \log(p(c_{ij}; \theta_{kl})) &= -\frac{1}{2} \sum_{k=1}^K \sum_{l=1}^L n_{kl} \left[ d_{kl} \log(a_{kl}) + (M - d_{kl}) \log(b_{kl}) \right. \\ &\quad \left. + \frac{1}{n_{kl}} \sum_{i=1}^n \sum_{j=1}^M z_{ik} w_{jl} (c_{ij} - \mu_{kl})^t \Phi^{1/2} Q_{kl} \Delta_{kl}^{-1} Q_{kl}^t \Phi^{1/2} (c_{ij} - \mu_{kl}) \right] \\ &\quad - \frac{nM}{2} \log(2\pi) \end{aligned}$$

Since the quantity  $(c_{ij} - \mu_{kl})^t \Phi^{1/2} Q_{kl} \Delta_{kl}^{-1} Q_{kl}^t \Phi^{1/2} (c_{ij} - \mu_{kl})$  is a scalar, it is equal to its trace:  $tr([(c_{ij} - \mu_{kl})^t \Phi^{1/2} Q_{kl}] \times [\Delta_{kl}^{-1} Q_{kl}^t \Phi^{1/2} (c_{ij} - \mu_{kl})]) = tr([\Delta_{kl}^{-1} Q_{kl}^t \Phi^{1/2} (c_{ij} - \mu_{kl})] \times [(c_{ij} - \mu_{kl})^t \Phi^{1/2} Q_{kl}])$ , consequently:

$$\begin{aligned} &\frac{1}{n_{kl}} \sum_{i=1}^n \sum_{j=1}^M z_{ik} w_{jl} (c_{ij} - \mu_{kl})^t \Phi^{1/2} Q_{kl} \Delta_{kl}^{-1} Q_{kl}^t \Phi^{1/2} (c_{ij} - \mu_{kl}) \\ &= \frac{1}{n_{kl}} \sum_{i=1}^n \sum_{j=1}^M z_{ik} w_{jl} tr(\Delta_{kl}^{-1} Q_{kl}^t \Phi^{1/2} (c_{ij} - \mu_{kl}) (c_{ij} - \mu_{kl})^t \Phi^{1/2} Q_{kl}) \\ &= tr(\Delta_{kl}^{-1} Q_{kl}^t \Phi^{1/2} [\frac{1}{n_{kl}} \sum_{i=1}^n \sum_{j=1}^M z_{ik} w_{jl} (c_{ij} - \mu_{kl})^t (c_{ij} - \mu_{kl})] \Phi^{1/2} Q_{kl}) \\ &= tr(\Delta_{kl}^{-1} Q_{kl}^t \Phi^{1/2} \Omega_{kl} \Phi^{1/2} Q_{kl}), \end{aligned}$$

where  $\Omega_{kl} = \frac{1}{n_{kl}} \sum_{i=1}^n \sum_{j=1}^M z_{ik} w_{jl} (c_{ij} - \mu_{kl})^t (c_{ij} - \mu_{kl})$  is the empirical covariance matrix of the curves of the block  $(kl)$ . Since the matrix  $\Delta_{kl}$  is diagonal, so we can write:

$$\begin{aligned} \frac{1}{n_{kl}} \sum_{i=1}^n \sum_{j=1}^M z_{ik} w_{jl} (c_{ij} - \mu_{kl})^t Q_{kl} \Delta_{kl}^{-1} Q_{kl}^t (c_{ij} - \mu_{kl}) &= \sum_{j=1}^{d_{kl}} \frac{q_{klj}^t \Phi^{1/2} \Omega_{kl} \Phi^{1/2} q_{klj}}{a_{klj}} \\ &\quad + \sum_{j=d_{kl}+1}^M \frac{q_{klj}^t \Phi^{1/2} \Omega_{kl} \Phi^{1/2} q_{klj}}{b_{kl}}, \end{aligned}$$

where  $q_{klj}$  is  $j$ th column of  $Q_{kl}$ .

Finally,

$$\begin{aligned}
H(\theta|\theta^{old}) &= \sum_{i,k} z_{ik}^{(h+1)} \log \alpha_k + \sum_{j,l} w_{jl}^{(h+1)} \log \beta_l \\
&- \frac{1}{2} \sum_{k,l} n_{kl} \left[ d_{kl} \log(a_{kl}) + (M - d_{kl}) \log(b_{kl}) \right. \\
&\left. + \sum_{j=1}^{d_{kl}} \frac{q_{klj}^t \Phi^{1/2} \Omega_{kl} \Phi^{1/2} q_{klj}}{a_{klj}} + \sum_{j=d_{kl}+1}^M \frac{q_{klj}^t \Phi^{1/2} \Omega_{kl} \Phi^{1/2} q_{klj}}{b_{kl}} \right] - \frac{nM}{2} \log(2\pi)
\end{aligned}$$

## A.2 Parameter $Q_{kl}$ update

We aim to maximize  $H(\theta|\theta^{old})$  under the constraint  $q_{klj}^t q_{klj} = 1$ , with  $q_{klj}$  the  $j$ th column of  $Q_{kl}$ . This is equivalent to look for a saddle point of the Lagrange function:

$$\mathcal{L} = -2H(\theta|\theta^{old}) - \sum_{j=1}^M \omega_{klj} (q_{klj}^t q_{klj} - 1)$$

where  $\omega_{klj}$  are Lagrange multipliers. The gradient of  $\mathcal{L}$  in relation to  $q_{klj}$  is:

$$\begin{aligned}
\nabla_{q_{klj}} \mathcal{L} &= \nabla_{q_{klj}} \left( \sum_{k=1}^K \sum_{l=1}^L n_{kl} \left[ \sum_{j=1}^{d_{kl}} \frac{q_{klj}^t \Phi^{1/2} \Omega_{kl} \Phi^{1/2} q_{klj}}{a_{klj}} + \sum_{j=d_{kl}+1}^M \frac{q_{klj}^t \Phi^{1/2} \Omega_{kl} \Phi^{1/2} q_{klj}}{b_{kl}} \right] \right. \\
&\left. - \sum_{j=1}^M \omega_{klj} (q_{klj}^t q_{klj} - 1) \right).
\end{aligned}$$

As a reminder, when  $W$  is symmetric, then  $\frac{\partial}{\partial x} (x-s)^T W (x-s) = 2W(x-s)$  and  $\frac{\partial}{\partial x} (x^T x) = 2x$  (cf. Petersen and Pedersen (2012)), so:

$$\nabla_{q_{klj}} \mathcal{L} = n_{kl} \left[ 2 \frac{\Phi^{1/2} \Omega_{kl} \Phi^{1/2}}{\sigma_{klj}} q_{klj} \right] - 2\omega_{klj} q_{klj}$$

where  $\sigma_{klj}$  is the  $j$ -th diagonal term of matrix  $\Delta_k$  ( $a_{klj}$  for  $j \leq d_{kl}$  and  $b_{kl}$  otherwise).

Thus,

$$\nabla_{q_{klj}} \mathcal{L} = 0 \Leftrightarrow \Phi^{1/2} \Omega_{kl} \Phi^{1/2} q_{klj} = \frac{\omega_{klj} \sigma_{klj}}{n_{kl}} q_{klj}.$$

$q_{klj}$  is the eigenfunction of  $\Phi^{1/2} \Omega_{kl} \Phi^{1/2}$  which match the eigenvalue  $\lambda_{klj} = \frac{\omega_{klj} \sigma_{klj}}{n_{kl}} = q_{klj}^t \Phi^{1/2} \Omega_{kl} \Phi^{1/2} q_{klj}$ . Since the vectors  $q_{klj}$  are eigenvectors of  $\Omega_{kl}$ , we have  $q_{klj}^t q_{klm} = 0$  if  $j \neq m$ . Reporting the value of  $\lambda_{klj}$  in  $H(\theta|\theta^{old})$  allows to see that maximizing  $H(\theta|\theta^{old})$  regarding  $q_{klj}$  is equivalent to minimize the quantity  $\sum_{k=1}^K \sum_{l=1}^L n_{kl} \sum_{j=1}^{d_{kl}} \lambda_{klj} \left( \frac{1}{a_{kl}} - \frac{1}{b_{kl}} \right)$  regarding to  $\lambda_{klj}$ . Knowing that  $\left( \frac{1}{a_{kl}} - \frac{1}{b_{kl}} \right) \leq 0$ ,  $\lambda_{kl}$  has to be as high as possible. therefore, the  $j$ -th column  $q_{klj}$  of matrix  $Q_{kl}$  is estimated by the eigen function associated to the  $j$ -th highest eigenvalue of  $\Phi^{1/2} \Omega_{kl} \Phi^{1/2}$ .

## A.3 Parameter $a_{kl}$ update

Partial derivative of  $H(\theta|\theta^{old})$  according to  $a_{kl}$  correspond to:

$$\begin{aligned}
\frac{\partial H(\theta|\theta^{old})}{\partial a_{kl}} &= -\frac{1}{2} n_{kl} \left( \frac{d_{kl}}{a_{kl}} - \sum_{j=1}^{d_{kl}} \frac{q_{klj}^t \Phi^{1/2} \Omega_{kl} \Phi^{1/2} q_{klj}}{a_{kl}^2} \right) \\
&= -\frac{1}{2} n_{kl} \left( \frac{d_{kl}}{a_{kl}} - \sum_{j=1}^{d_{kl}} \frac{\lambda_{klj}}{a_{kl}^2} \right)
\end{aligned}$$

The prerequisite  $\frac{\partial H(\theta|\theta^{old})}{\partial a_{kl}} = 0$  implies:

$$\frac{n_{kl}d_{kl}}{a_{kl}} = \frac{n_{kl}}{a_{kl}^2} \sum_{j=1}^{d_{kl}} \lambda_{klj}$$

$$\Leftrightarrow a_{kl} = \frac{1}{d_{kl}} \sum_{j=1}^{d_{kl}} \lambda_{klj}$$

with  $\lambda_{kl}$  the eigen values of block  $kl$ .

#### A.4 Parameter $b_{kl}$ update

Partial derivative of  $H(\theta|\theta^{old})$  according to  $b_{kl}$  correspond to:

$$\frac{\partial H(\theta|\theta^{old})}{\partial b_{kl}} = -\frac{1}{2} \left[ \frac{M - d_{kl}}{b_{kl}} - \sum_{j=d_{kl}+1}^M \frac{q_{klj}^t \Phi^{1/2} \Omega_{kl} \Phi^{1/2} q_{klj}}{b_{kl}^2} \right]$$

The prerequisite  $\frac{\partial H(\theta|\theta^{old})}{\partial b_{kl}} = 0$  implies:

$$\frac{M - d_{kl}}{b_{kl}} = \sum_{j=d_{kl}+1}^M \frac{q_{klj}^t \Phi^{1/2} \Omega_{kl} \Phi^{1/2} q_{klj}}{b_{kl}^2}$$

$$\Leftrightarrow b_{kl} = \frac{1}{M - d_{kl}} \left[ \text{tr}(\Phi^{1/2} \Omega_{kl} \Phi^{1/2}) - \sum_{j=1}^{d_{kl}} \lambda_{klj} \right]$$

#### A.5 Distribution of weeks by cluster

Table 2: Number of weeks by year by cluster.

Cluster/Year	2013	2014	2015	2016	2017	2018
1	16	12	17	11	9	7
2	8	9	8	9	7	11
3	11	10	7	12	7	18
4	9	10	11	7	15	8
5	5	9	3	11	8	6
6	4	3	7	3	7	3

Table 3: Number of weeks by month by cluster.

Cluster/Month	Jan	Feb	Mar	Apr	May	Jun	Jul	Aug	Sep	Oct	Nov	Dec
1	15	12	6	3	1	0	0	0	1	11	12	23
2	0	0	0	1	3	14	22	15	7	1	0	0
3	3	4	14	14	17	7	2	0	3	6	7	2
4	0	0	5	9	6	9	5	7	15	11	2	0
5	13	14	4	3	0	0	0	0	0	2	6	6
6	1	0	2	1	5	1	3	9	5	1	3	1

Table 4: Number of weeks by season by cluster.

<i>Cluster/Season</i>	Winter	Spring	Summer	Autumn
1	38	3	0	35
2	0	11	43	1
3	13	34	7	12
4	4	24	22	19
5	26	4	0	11
6	1	8	13	5

## References

- (2013). Review of evidence on health aspects of air pollution - REVIHAAP Project. Technical report, WHO Regional Office for Europe, Copenhagen, Denmark.
- (2016). *Outdoor air pollution*, Volume 109 of *IARC Monogr Eval Carcinog Risks Hum*. IARC.
- Akaike, H. (1974). A new look at the statistical model identification. *IEEE Transactions on Automatic Control* 9, 716–723.
- Banerjee, A., I. Dhillon, J. Ghosh, S. Merugu, and D. S. Modha (2007). A generalized maximum entropy approach to bregman co-clustering and matrix approximation. *Journal of Machine Learning Research* 8(Aug), 1919–1986.
- Benbrahim-Tallaa L, Baan RA, G. Y. L.-S. B. E. G. F. B. V. e. a. (2012). Carcinogenicity of diesel-engine and gasoline-engine exhausts and some nitroarenes. *The Lancet Oncology* 13, 663–664.
- Bhatia, P., S. Iovleff, and G. Govaert (2014, December). blockcluster: An R Package for Model Based Co-Clustering. working paper or preprint.
- Biernacki, C., G. Celeux, and G. Govaert (2000). Assessing a mixture model for clustering with the integrated completed likelihood. *IEEE Trans. PAMI* 22, 719–725.
- Bouveyron, C., L. Bozzi, J. Jacques, and F.-X. Jollois (2017, December). The Functional Latent Block Model for the Co-Clustering of Electricity Consumption Curves. *Journal of the Royal Statistical Society: Series C Applied Statistics*.
- Bouveyron, C., G. Celeux, T. B. Murphy, and A. E. Raftery (2019). *Model-Based Clustering and Classification for Data Science: With Applications in R*. Cambridge University Press.
- Bouveyron, C., L. Cheze, J. Jacques, P. Martin, and A. Schmutz (2020). Clustering multivariate functional data in group-specific functional subspaces. *Computational Statistics*, in press.
- Bouveyron, C., E. Come, and J. Jacques (2015). The discriminative functional mixture model for the analysis of bike sharing systems. *Annals of Applied Statistics* 9(4), 1726–1760.
- Bouveyron, C., E. Côme, and J. Jacques (2015). The discriminative functional mixture model for a comparative analysis of bike sharing systems. *Annals of Applied Statistics*, in press.
- Chamroukhi, F. and C. Biernacki (2017, July). Model-Based Co-Clustering of Multivariate Functional Data. In *ISI 2017 - 61st World Statistics Congress*, Marrakech, Morocco.
- Corneli, M., C. Bouveyron, and P. Latouche (2019, January). Co-Clustering of ordinal data via latent continuous random variables and a classification EM algorithm. working paper or preprint.
- Delaigle, A. and P. Hall (2010). Defining probability density for a distribution of random functions. *The Annals of Statistics* 38, 1171–1193.

- Dempster, A. P., N. M. Laird, and D. B. Rubin (1977). Maximum likelihood from incomplete data via the EM algorithm. *Journal of the Royal Statistical Society. Series B. Methodological* 39(1), 1–38.
- George, T. and S. Merugu (2005). A scalable collaborative filtering framework based on co-clustering. In *Data Mining, Fifth IEEE international conference on*, pp. 4–pp. IEEE.
- Govaert, G. and M. Nadif (2013). *Co-Clustering* (1st ed.). Wiley-IEEE Press.
- Hamra GB, Guha N, C. A. L. F.-R.-N. O. S. J. e. a. (2014). Outdoor particulate matter exposure and lung cancer: a systematic review and meta-analysis. *Environ Health Perspectives* 112, 906–911.
- Jacques, J. and C. Biernacki (2018, July). Model-Based Co-clustering for Ordinal Data. *Computational Statistics and Data Analysis* 123, 101–115.
- Jacques, J. and C. Preda (2013). Funclust: a curves clustering method using functional random variable density approximation. *Neurocomputing* 112, 164–171.
- Jacques, J. and C. Preda (2014a). Functional data clustering: a survey. *Advances in Data Analysis and Classification* 8(3), 231–255.
- Jacques, J. and C. Preda (2014b). Model based clustering for multivariate functional data. *Computational Statistics and Data Analysis* 71, 92–106.
- Keribin, C., G. Govaert, and G. Celeux (2010). Estimation d'un modèle à blocs latents par l'algorithme SEM. In *42èmes Journées de Statistique*, Marseille, France, France.
- Laclau, C., I. Redko, B. Matei, Y. Bennani, and V. Brault (2017, August). Co-clustering through Optimal Transport. In *34th International Conference on Machine Learning*, Volume 70 of *Proceedings of the 34th International Conference on Machine Learning*, Sydney, Australia, pp. 1955–1964. Proceedings of Machine Learning Research.
- Lelieveld, J., E. J. F. M. e. a. (2015). The contribution of outdoor air pollution sources to premature mortality on a global scale. *Nature* 525, 367–371.
- Mathilde Pascal, Perrine de Crouy Chanel, V. W. M. C. C. T. M. B. M. B. A. C. L. P. S. H. S. G. A. L. T. E. C. A. U. P. B. S. M. (2016). The mortality impacts of fine particles in france. *Science of the Total Environment* 571, 416–425.
- Menut, L., B. B. K. D. B. M. B. N. C. A. C. I. C. G. F. G. H. A. M. S. M. F. M. J.-L. P. I. S. G. T. S. V. M. V. R. and M. G. Vivanco (2013). Chimere 2013: a model for regional atmospheric composition modelling. *Geosci. Model Dev.* 6, 981–1028.
- Nadif, M. and G. Govaert (2008). Algorithms for model-based block gaussian clustering. In *Proceedings of The 2008 International Conference on Data Mining, DMIN 2008, July 14-17, 2008, Las Vegas, USA, 2 Volumes*, pp. 536–542.
- Petersen, K. B. and M. S. Pedersen (2012, nov). The matrix cookbook. Version 20121115.
- Ramsay, J. O. and B. W. Silverman (2005). *Functional data analysis* (Second ed.). Springer Series in Statistics. New York: Springer.
- Rand, W. M. (1971). Objective criteria for the evaluation of clustering methods. *Journal of the American Statistical Association* 66(336), 846–850.
- Schwarz, G. (1978). Estimating the dimension of a model. *The Annals of Statistics* 6(2), 461–464.
- Selosse, M., J. Jacques, and C. Biernacki (2019, October). Model-based co-clustering for mixed type data. *Computational Statistics and data analysis*.
- Slimen, Y. B., S. Allio, and J. Jacques (2018). Model-Based Co-clustering for Functional Data. *Neurocomputing* 291, 97–108.
- Wang, S. and A. Huang (2017). Penalized nonnegative matrix tri-factorization for co-clustering. *Expert Systems with Applications* 78, 64–73.